

Molecular Simulation Study of Water Interactions with Oligo (Ethylene Glycol)-Terminated Alkanethiol Self-Assembled Monolayers

Jie Zheng, Lingyan Li, Shenfu Chen, and Shaoyi Jiang*

Department of Chemical Engineering, University of Washington, Seattle, Washington 98195

Received December 11, 2003. In Final Form: July 8, 2004

Molecular simulations were performed to study a system consisting of protein (e.g., lysozyme) and self-assembled monolayers (SAMs) terminating with different chemical groups in the presence of explicit water molecules and ions. Mixed SAMs of oligo (ethylene glycol) $[S(CH_2)_4(OCH_2CH_2)_4OH]$, (OEG) and hydroxyl-terminated SAMs $[S(CH_2)_4OH]$ with a mole fraction of OEG at $\chi_{OEG} = 0.2, 0.5, 0.8,$ and 1.0 were used in this study. In addition, methyl-terminated SAMs $[S(CH_2)_{11}CH_3]$ were also studied for comparison. The structural and dynamic behavior of hydration water, the flexibility and conformation state of SAMs, and the orientation and conformation of protein were examined. Simulation results were compared with those of experiments. It appears that there is a correlation between OEG surface resistance to protein adsorption and the surface density of OEG chains, which leads to a large number of tightly bound water molecules around OEG chains and the rapid mobility of hydrated SAM chains.

I. Introduction

Surface resistance to protein adsorption is currently a subject of great interest, with potential applications such as blood-contacting devices, implanted devices, contact lenses, substrates for cell culture, and coatings on boat hulls.^{1–3} Experimental studies of protein interactions with surfaces have been performed extensively over the past years. A number of surfaces that present oligo (ethylene glycol) (OEG),⁴ carboxylic anhydride,⁵ and phosphorylcholine⁷ and its derivative⁶ groups have been synthesized and identified in their ability to reduce protein adsorption. Among them, the OEG-terminated self-assembled monolayers (SAMs), $S(CH_2)_m(OCH_2CH_2)_nOR$ ($R = H, CH_3$), are widely used and studied.⁸ However, the mechanism for OEG SAMs to resist protein adsorption is not fully understood due to the complex interplay of various interactions among proteins, solvents, and surfaces. Protein behavior on surfaces is determined not only by protein structures (e.g., size and shape) but also by surface properties (e.g., charge and hydrophobicity). More importantly, the structure and conformation of water molecules near surfaces may play an important role on protein adsorption. Whitesides et al.² showed that surfaces resisting adsorption of proteins exhibited four common molecular-level features²—(i) hydrophilic, (ii) electrically neutral, (iii) hydrogen bond acceptors, and (iv) not hydrogen bond donors.

De Gennes and co-workers⁹ reported the first theoretical studies of the resistance of poly(ethylene oxide) (PEO) polymers to protein adsorption. They concluded that steric repulsion resulting from the compression of PEO chains as protein approaches the surface was mainly responsible for prevention of protein adsorption. It was predicted that the longer chain lengths and higher surface densities lead to better protein resistance. Szeleifer et al.¹⁰ improved the model of De Gennes et al.⁹ using the single chain mean field (SCMF) theory. They found that polymers grafted to a hydrophobic surface reduced protein adsorption because they blocked adsorption sites for proteins. In the Szeleifer model, while surface density was also an important factor in its ability to prevent protein adsorption, chain length had a weak effect on protein adsorption. Thus, the Szeleifer model is able to interpret experimental results,² for which short OEG groups were used. While De Gennes and Szeleifer models provide some insight regarding the mechanism of surface resistance to protein adsorption, their models do not provide molecular-level information. In their work, the protein was modeled as a structureless, spherical particle, while water was treated as a continuous medium in the De Gennes model or as a homogeneous spherical noninteracting molecule in the Szeleifer model. While simplified models allow simulations to be performed in the time scale of seconds, the detailed conformational change of a protein and polymer chains was ignored. Furthermore, it has been suggested^{2,11–15} that the formation of tightly bound water molecules at the protein/SAM interface is very important for protein nonfouling

* Author to whom correspondence should be addressed.

(1) *Proteins at interfaces II, Fundamentals and Applications*; Horbett, T. A.; Brash, J. L., Eds.; ACS Symposium Series, 602; American Chemical Society: Washington, DC, 1995.

(2) Ostuni, E.; Chapman, R. G.; Holmlin, R. E.; Takayama, S.; Whitesides, G. M. *Langmuir* **2001**, *17*, 5605.

(3) Kane, R. S.; Deschatelets, P.; Whitesides, G. M. *Langmuir* **2003**, *19*, 2388.

(4) *Poly(ethylene glycol) Chemistry*; Harris, J. M., Ed.; Plenum Press: New York, 1992.

(5) Chapman, R. G.; Ostuni, E.; Liang, M. N.; Meluleni, G.; Kim, E.; Yan, L.; Pier, G.; Warren, H. S.; Whitesides, G. M. *Langmuir* **2001**, *17*, 1225.

(6) Tegoulia, V. A.; Rao, W.; Kalambar, A. T.; Rabolt, J. F.; Cooper, S. L. *Langmuir* **2001**, *17*, 4396.

(7) Murphy, E. F.; Lu, J. R.; Brewer, J.; Russell, J.; Penfold, J. *Langmuir* **1999**, *15*, 1313.

(8) Rabinow, B. E.; Ding, Y. S.; Qin, C.; McHalsky, M. L.; Schneider, J. H.; Ashline, K. A.; Shelbourn, T. L.; Albrecht, R. M. *J. Biomater. Sci., Polym. Ed.* **1994**, *6*, 91–109.

(9) Jeon, S. I.; Lee, J. H.; Andrade, J. D.; De Gennes, P. G. *J. Colloid Interface Sci.* **1991**, *142*, 149.

(10) McPherson, T.; Kidane, A.; Szeleifer, I.; Park, K. *Langmuir* **1998**, *14*, 176.

(11) Luck, Y. Y.; Kato, M.; Mrksich, M. *Langmuir* **2000**, *16*, 9604.

(12) Ostuni, E.; Chapman, R. G.; Liang, M. N.; Meluleni, G.; Pier, G.; Ingber, D. E.; Whitesides, G. M. *Langmuir* **2001**, *17*, 6336.

(13) Pertsin, A. J.; Grunze, M. *Langmuir* **2000**, *16*, 8829.

(14) Pertsin, A. J.; Grunze, M.; Garbuzova, I. A. *J. Phys. Chem. B* **1998**, *102*, 4918.

(15) Harder, P.; Grunze, M.; Dahint, R.; Whitesides, G. M.; Laibinis, P. E. *J. Phys. Chem. B* **1998**, *102*, 426.

mechanism. However, explicit water molecules were not included in those two models. Recently, Grunze et al.^{13–15} performed grand canonical Monte Carlo (GCMC) simulations to study the interactions of water molecules with OEG-terminated alkanethiol SAMs on gold and silver substrates. They attributed OEG-SAMs with helical conformation on gold (h-SAM) to reduce protein adsorption, while those SAMs with and all zigzag conformation on silver (t-SAM) enhance protein adsorption. Their results showed that more water molecules penetrated into h-SAM than t-SAM to form hydrogen bonds with OEG chains, leading to the prevention of protein adsorption on the surfaces. However, their simulations involved only water and SAMs but not protein. So far, few molecular simulation studies of protein interactions with surfaces have been reported. Recently, Klein and co-workers^{16,17} performed molecular dynamics (MD) simulation studies of the adsorption of cytochrome *c* on both hydrophobic (–CH₃) and hydrophilic (–SH) SAM surfaces. They found that the protein and water molecules were excluded from the hydrophobic SAMs but partially penetrated into the hydrophilic SAMs.¹⁷ Their simulations were performed either in the absence¹⁶ or in the presence of a limited amount of water molecules (i.e., 500 water molecules)¹⁷ to model some degrees of hydration of the protein.

In this paper, molecular simulations were performed to study a system consisting of protein (e.g., lysozyme) and self-assembled monolayers (SAMs) terminating with different chemical groups [e.g., CH₃, OH, and (OCH₂CH₂)₄OH] in the presence of explicit water molecules and ions. The surface density of (OCH₂CH₂)₄OH groups was controlled by adjusting the surface composition of mixed SAMs of SH(CH₂)₄(OCH₂CH₂)₄OH and SH(CH₂)₄OH. While it is difficult to prepare high-density and well-ordered OEG-SAMs experimentally, simulations will allow one to systematically control SAM surface density and packing. This work will shed light on the protein nonfouling mechanism at the atomic level and may help guide the design of better biocompatible materials.

II. Simulation Model and Methodology

Model Systems. In this work, we chose SAM surfaces terminating with four repeated units of OEG functional groups, i.e., S(CH₂)₄(OCH₂CH₂)₄OH (OEG-SAM), to study the nonfouling mechanism. SAMs terminating with methyl groups, e.g., S(CH₂)₉CH₃ (CH₃-SAM), are also studied for comparison. A set of OEG-terminated alkanethiolates in pure OEG-SAMs were randomly selected and replaced by the shorter hydroxyl-terminated alkanethiolates, i.e., S(CH₂)₄OH, to form mixed SAMs of S(CH₂)₄(OCH₂CH₂)₄OH and S(CH₂)₄OH with a mole fraction of S(CH₂)₄(OCH₂CH₂)₄OH at $\chi_{\text{OEG}} = 1.0, 0.8, 0.5, \text{ and } 0.2$. Each system in our simulations comprises a single lysozyme with SAMs in the presence of explicit solvent water molecules and counterions.

A single chain used in the OEG-SAMs and the CH₃-SAMs was built using the CHARMM program and then was energy minimized in a vacuum. Early electronic diffraction studies of alkanethiol monolayers on Au(111)¹⁸ have shown a hexagonal symmetry of sulfur atoms with a nearest-neighbor spacing of 0.497 nm. A scanning tunneling microscopy study of *n*-alkyl thiol on Au(111)¹⁹ has shown that sulfur atoms are constrained in the ($\sqrt{3} \times \sqrt{3}$)R30° hexagonal lattice positions. Thus, the SAM surfaces used in our simulations were an 11 × 12 array of the minimized single chain with a ($\sqrt{3} \times \sqrt{3}$)R30° lattice structure and

a sulfur–sulfur spacing of 0.497 nm. These chains were initially tilted by ~30° from the *z* axis perpendicular to the Au(111) surface. The initial structure of the CH₃-SAM chains has a zigzag configuration, while the OEG-SAMs have a helical configuration. The molecular area of the CH₃-SAMs is 21.2 Å²/chain. In the case of the OEG-SAMs, the molecule area is 27.4 Å²/chain.

Lysozyme is often used in model studies of adsorption of proteins to surfaces since its structure, dynamics, and folding have been studied extensively by a wide range of experimental and theoretical techniques.²⁰ The X-ray crystal structure of lysozyme, comprising 129 amino acids, was taken from the Protein Data Bank (entry code 7LYZ). Polar and aromatic hydrogens were explicitly added to the protein. The amino acids histidine (HIS), arginine (ARG), and lysine (LYS) were protonated while glutamate (GLU) and aspartate (ASP) were taken to be deprotonated; four disulfide bonds were added; the N terminus (NH₃⁺) and the C terminus (COO[–]) were assigned a charge state of +1e and –1e, respectively; all other amino acid side chains were kept neutral. This procedure leads to a net charge of +8e on the protein at pH 7.

The CHARMM22 parameter set, an all-atom potential force field, was used to model the protein and the CH₃-terminated SAMs. Water molecules were treated as the three-site point charge model (TIP3P). For OEG chains, a force field^{23,24} based on ab initio calculation results was used in order to correctly describe the helical structure of OEG in solution. A number of quantum mechanics (QM) and MD studies^{22–27} reported previously the force fields for poly(ethylene oxide) (PEO), i.e., –(CH₂CH₂O)_{*n*}–, a repeated unit in OEG-SAMs. Smith and co-workers^{23,24} developed an empirical force field for PEO to describe the PEO-PEO and PEO-water interactions using ab initio electronic structure calculations. This model can reproduce very well the helical structure of PEO in solution. Thus, the force field parameters for PEO as reported by Smith et al.^{23,24} were adopted in this work except for some changes as follows. In the Smith's model, van der Waals (VDW) interactions were described by the Buckingham potential, $\sum A \exp(-Br_{ij}) - Cr_{ij}$. The parameters of the Lennard-Jones (LJ) 12–6 potential used in CHARMM and our simulation program were obtained by fitting the Buckingham potential with the least-squares method by Tasaki.²⁶ Similarly, the parameters of the torsion potential used in the Smith's model, $\sum k_{\phi}[\cos n(\phi - \delta)]$, were also adjusted to reproduce the torsion potential within the CHARMM format, $\sum k_{\phi}[1 + \cos(n\phi - \delta)]$. In addition, cross LJ parameters involving water and OEG-SAMs were modified to yield better agreement with those results from quantum chemical calculations at the HF/aug-cc-pvDz level.²⁴ Further details about the model of PEO and its force field parameters are given in refs 23, 24, and 26.

The potential energy function used in our simulations consists of bond, Urey-Bradley (UB), angle, dihedral, and improper terms, as well as nonbonded VDW and Coulombic interactions. The complete form of the energy function is given by

$$U = \sum_{\text{bonds}} k_b(b - b_0)^2 + \sum_{\text{UB}} k_{\text{UB}}(r - r_0)^2 + \sum_{\text{angles}} k_{\theta}(\theta - \theta_0)^2 + \sum_{\text{dihedrals}} k_{\phi}[1 + \cos(n\phi - \delta)] + \sum_{\text{impropers}} k_{\chi}(\chi - \chi_0)^2 + \sum_{\text{vdW}} \epsilon_{ij} \left[\left(\frac{R_{\text{min},ij}}{r_{ij}} \right)^{12} - 2 \left(\frac{R_{\text{min},ij}}{r_{ij}} \right)^6 \right] + \sum_{\text{Coulombic}} \frac{q_i q_j}{4\pi\epsilon_0 r_{ij}} \quad (1)$$

The first five terms in the potential energy function describe the

(20) Smith, L. J.; Mark, A. E.; Dobson, C. M.; van Gunsteren, W. F. *Biochemistry* **1995**, *34*, 10918.

(21) Dubois, L. H.; Nuzzo, R. G. *Annu. Rev. Phys. Chem.* **1992**, *43*, 437.

(22) Sorensen, R. A.; Liao, W. B.; Kesner, L.; Boyd, R. H. *Macromolecules* **1988**, *21*, 200.

(23) Smith, G. D.; Jaffe, R. L.; Yoon, D. Y. *J. Phys. Chem.* **1993**, *97*, 12752.

(24) Smith, G. D.; Borodin, O.; Bedrov, D. *J. Comput. Chem.* **2002**, *23*, 1480.

(25) Neyertz, S.; Brown, D.; Thomas, J. O. *J. Chem. Phys.* **1994**, *101*, 10064.

(26) Tasaki, K. *J. Am. Chem. Soc.* **1996**, *118*, 8459.

(27) Tasaki, K. *Macromolecules* **1996**, *29*, 8922.

(16) Tobias, D. J.; Mar, W.; Blasie, J. K.; Klein, M. L. *Biophys. J.* **1996**, *71*, 2933.

(17) Nordgren, C. E.; Tobias, D. J.; Klein, M. L.; Blasie, J. K. *Biophys. J.* **2002**, *83*, 2906.

(18) Widrig, C. A.; Alves, C. A.; Porter, M. D. *J. Am. Chem. Soc.* **1991**, *113*, 2805.

(19) Takano, H.; Kenseth, J. R.; Wong, S.; O'Brien, J. C.; Porter, M. D. *Chem. Rev.* **1999**, *99*, 2845.

bonded interactions, in which k_b , k_{UB} , k_a , k_ϕ , and k_γ are the bond, UB, angle, dihedral, and improper force constants, respectively; b_0 , r_0 , θ_0 , δ , and γ_0 are the equilibrium values for bond length, UB 1-3 distance, bond angle, dihedral angle, and improper angle, respectively. The last two terms in the potential energy function are for nonbonded interactions, where ϵ_{ij} is the LJ well depth, R_{\min} is the distance at the LJ minimum, q_i is the partial atomic charge, and r_{ij} is the distance between atoms i and j . All cross LJ parameters were calculated using the geometry combining rule for $\epsilon_{ij} = \sqrt{\epsilon_i \epsilon_j}$ and arithmetic combining rule for $R_{\min ij} = \{(R_{\min i} + R_{\min j})/2\}$, respectively.

Simulation Methodology. We performed molecular simulations according to the following two-step protocol. First, we carried out a series of Metropolis MC simulations in the canonical ensemble (NVT) at $T = 300$ K to determine the orientation of lysozyme at different SAM interfaces in a continuum distance-dependent dielectric medium. The systems taken from the MC phase were then immersed in the explicit water solvent and were simulated using the MD approach.

For the MC phase, lysozyme was manually placed at various separation distances (5–10 Å) with respect to surfaces with a random orientation. For each of the five systems, we generated several initial starting configurations with different separations and orientations of lysozyme relative to the surfaces. Starting from these initial configurations of each system, lysozyme was moved by either a uniform random displacement or a rotation about an arbitrary axis with the acceptance rate of $\sim 50\%$. The probability of a move being accepted is given by the Metropolis criteria. In all MC simulations, water was treated as an implicit solvent continuum model, the SAM surfaces were fixed in the xy plane, and lysozyme was modeled as a rigid molecule. With the model described above, only VDW and Coulombic nonbonded interactions between the protein and the SAM surfaces were involved. Simulations were carried out for 10^5 MC steps for the each initial condition of the five systems.

Following MC simulations, the optimal orientation of lysozyme at the SAM interfaces was obtained and lysozyme was placed ~ 5.0 Å above the SAM surfaces. Then, lysozyme and the SAM surfaces were immersed in a pre-equilibrated box of TIP3P water molecules with a density of 1 g/cm³. Counterions (1 sodium and 9 chlorines) were added to balance system charges. Any water molecule that is close to the protein or the SAMs within 3.0 Å was then removed. The system with the protein, water, SAMs, and counterions was initially minimized in energy for 4000 cycles using the conjugate gradient algorithm to remove any bad contacts between molecules. This minimized system was then gradually heated from 50 to 300 K with 50 K increments in a short MD run of 20 000 steps of 1.0 fs with harmonically constraining the backbone atoms of the protein and the SAMs to their initial positions. This heating process allowed for the initial relaxation of water molecules around the protein and the SAM surfaces. For the equilibrium MD part, the starting configuration of the protein, water, SAMs, and counterions was taken from the final frame of the heating MD simulation, as shown in Figure 1. Initial velocities were assigned with a Maxwell–Boltzmann distribution at 300 K. Each simulation system was placed in a rectangular box of $5.5 \times 5.2 \times 6.4$ nm³. All coordinates of sulfur atoms were fixed in the xy plane during MD simulations. The periodic boundary condition and minimum image convention were applied to the x and y directions only. The simulation cell was confined in the z direction by two hard walls. The velocity Verlet method was used for the integration of the Newton's equation. We used the NVT ensemble with a time step of 1.0 fs. The system was maintained at a constant temperature of 300 K using the Berendsen thermostat with a time constant of 0.1 ps. Since bond vibration is very fast, any covalent bond involving hydrogen atoms was kept rigid using the RATTLE method with a geometric tolerance of 0.0001 . The switch function was used to calculate VDW interactions between 0.8 and 1.0 nm. The force-shifting function was used for the long-range electrostatic interactions at a cutoff distance of 1.2 nm. The atom-based force-shifting function and the particle-mesh Ewald technique generated stable and very similar nanosecond trajectories for double-stranded DNA.³⁴ The cell-based neighbor

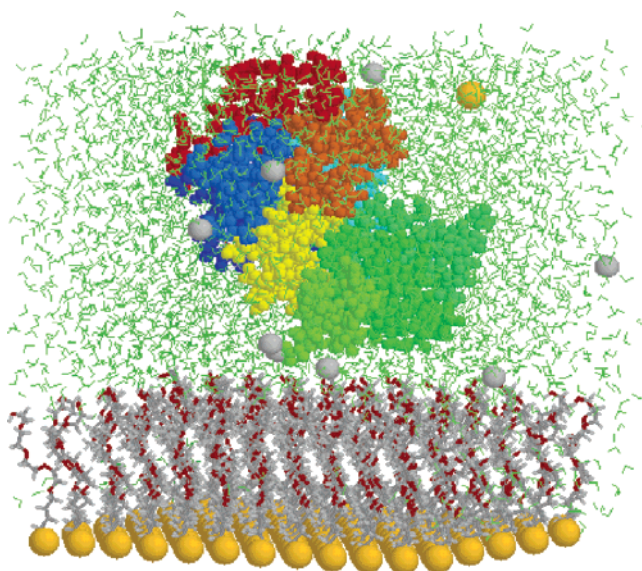


Figure 1. Illustration of protein (lysozyme) on OEG-terminated SAMs/Au (111) in the presence of explicit water molecules and counterions.

list with a cutoff range of 1.32 nm was used to reduce computational time for energy and energy-derivative calculations, which typically consume $\sim 90\%$ of computational time. Speed is enhanced approximately by a factor of 4 as compared with the group-based or atom-based neighbor list. The cell-based neighbor list was updated automatically if any atom in the list was moved by more than $(1.32 - 1.2)/2 = 0.06$ nm. During simulations, configurations were saved every 1.0 ps after 1 ns for analysis. The total length of an MD simulation run is about 1.5 ns. The total number of atoms in our simulation systems is about $16\,000$. All simulations were performed on a 16-node Linux cluster Intel x86 (CPU 1.0 GHz) using our BIOSUF program. We developed this generalized molecular simulation program for the study of a protein at biological interfaces. All initial structures were built using the CHARMM program.

III. Results and Discussion

We first performed MC simulations to determine protein orientation and then performed MD simulations to study the interactions among protein, OEG- or CH₃-SAMs, water molecules, and ions. The focus of this work will be on the behavior of bound water molecules around OEG chains and the flexibility of OEG chains, while protein orientation and conformation will be also discussed.

Protein Orientation. MC simulations were performed from different initial lysozyme orientations and positions. The lowest-energy conformations for lysozyme on the CH₃-SAM and OEG-SAM surfaces were identified. For the CH₃-SAM surface, the nearest separation distance between the protein and the surface was ~ 0.20 nm, in which the hydrophobic residues GLY67, PRO79, and ILE88 were closest to the surface, as shown in Figure 2a. For various OEG-SAM surfaces, lysozyme exhibited a similar orientation, i.e., hydrophilic residues ASN77 and ARG68 were closest to the surfaces with a separation distance of ~ 0.18 nm, as shown in Figure 2b. The V-shape

(29) Harris, D. J.; Bonagamba, T. J.; Hong, M.; Schmidt-Rohr, K. *Macromolecules* **2000**, *33*, 3375.

(30) Vanderah, D. J.; Valincius, G.; Meuse, C. W. *Langmuir* **2002**, *18*, 4674.

(31) Zhang, Q.; Zheng, J.; Shevade, A. V.; Zhang, L.; Gehrke, S. H.; Heffelfinger, G. S.; Jiang, S. *J. Chem. Phys.* **2002**, *117*, 808.

(32) Shevade, A. V.; Jiang, S.; Gubbins, K. E. *Mol. Phys.* **1999**, *97*, 1139.

(33) Bandyopadhyay, S.; Tarek, M.; Lynch, M. L.; Klein, M. L. *Langmuir* **2000**, *16*, 942.

(34) Norberg, J.; Nilsson, L. *Rev. Biophys.* **2003**, *36*, 3.

(28) Dadarlat, V. M.; Post, C. B. *J. Phys. Chem. B* **2001**, *105*, 715.

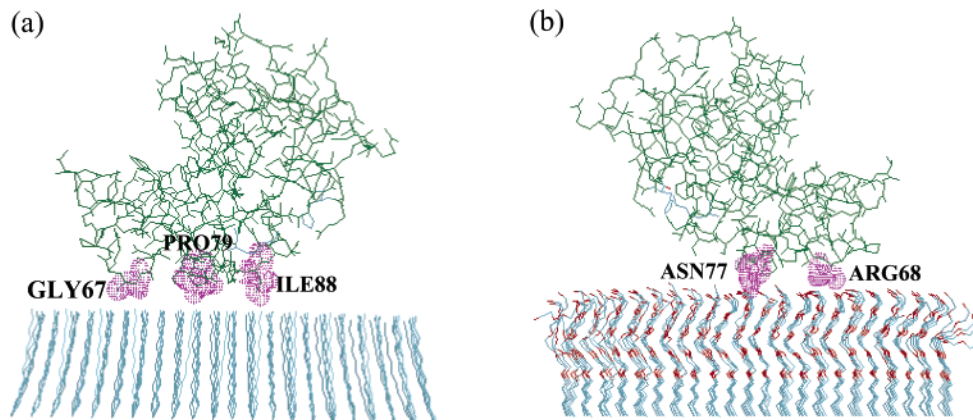


Figure 2. Snapshots of the optimal orientation of protein on (a) the CH₃-SAM surface and (b) the OEG-SAM surface. The residues with the closest distance to the surface are labeled.

Table 1. Simulation Results for Protein and the SAMs^a

| model system | CH ₃ -SAMs | OEG-SAMs | | | |
|-------------------------|-----------------------|--------------|--------------|--------------|--------------|
| | | 100% | 80% | 50% | 20% |
| | | Protein | | | |
| all-atom RMSD (Å) | 2.03 ± 0.07 | 1.88 ± 0.04 | 1.87 ± 0.06 | 1.85 ± 0.02 | 1.84 ± 0.05 |
| C ^α RMSD (Å) | 1.41 ± 0.08 | 1.35 ± 0.04 | 1.33 ± 0.08 | 1.31 ± 0.06 | 1.28 ± 0.03 |
| radius of gyration (Å) | 14.34 ± 0.06 | 14.21 ± 0.03 | 14.18 ± 0.05 | 14.19 ± 0.03 | 14.15 ± 0.06 |
| | | SAM Surfaces | | | |
| RMSD (Å) | 0.68 ± 0.03 | 0.93 ± 0.01 | 1.29 ± 0.03 | 1.25 ± 0.02 | 1.10 ± 0.04 |
| ⟨θ _s ⟩ (deg) | 33.26 ± 0.32 | 6.52 ± 0.14 | 9.70 ± 0.14 | 16.79 ± 0.23 | 14.46 ± 0.48 |
| ⟨θ _m ⟩ (deg) | 33.54 ± 0.31 | 28.65 ± 0.08 | 34.07 ± 0.10 | 38.96 ± 0.14 | 39.45 ± 0.39 |

^a The error corresponds to the standard deviations.

of lysozyme was oriented away from the surface for all cases studied.

Protein Conformation. The effect of surface chemistry on the mobility and size of the adsorbed protein is of interest to us in this work. The conformational changes of the protein during MD simulations were monitored by the root-mean-square derivations (RMSD) with its X-ray structure as a reference. The RMSD value, a measure of molecular mobility, is calculated by translating and rotating the coordinates of the instantaneous structure to superimpose the reference structure with a maximum overlap. The RMSD is defined as

$$\text{RMSD} = \sqrt{\frac{\sum_{i=1}^N m_i (r_i - r_i^0)^2}{\sum_{i=1}^N m_i}} \quad (2)$$

where m_i is the mass of atom i . r_i and r_i^0 are the coordinates of atom i at a certain instance during MD simulations and at its reference state, respectively. In all simulations, the RMSD of the protein rose steadily to reach a stable value after 1 ns. The positional deviation of C^α atoms is usually smaller than that of all atoms since hydrogen atoms often exhibit larger mobility during simulations. As shown in Table 1, for the OEG-SAM systems, the mobility of the protein was ~0.186 nm for all atoms and ~0.132 nm for C^α atoms. For the CH₃-SAM system, the RMSD was ~8% larger in structural drift than for the OEG-SAM systems due to strong hydrophobic forces. In general, higher hydration will lead to a smaller RMSD of a protein. This is consistent with experimental observation that the deviation of the mean structure of protein in vacuo is smaller than in solution.

The radius of gyration (R_{gyr}) for a protein is defined as the mass-weighted geometric mean of the distance of each atom from the protein's center of mass.

$$R_{\text{gyr}} = \sqrt{\frac{\sum_{i=1}^N m_i (r_i - r_{\text{com}})^2}{\sum_{i=1}^N m_i}} \quad (3)$$

where r_{com} is the center of mass of a protein. In Table 1, we observed that the overall size of lysozyme measured by the R_{gyr} was very stable around 1.425 nm for different SAM surfaces. The R_{gyr} of the protein was about 1% larger in the CH₃-SAMs than in the OEG-SAMs. The protein was smaller when fully hydrated than when not hydrated. Similar behavior was observed by Klein and co-workers¹⁷ when a cytochrome *c* was attached to a methyl-terminated or a hydroxyl-terminated SAM surface.

SAM Conformation. The conformation of the SAMs plays an important role on protein adsorption. To characterize the conformation of the SAMs, the mean system tilt (θ_s) and the molecular tilt (θ_m) were used in this work. The mean system tilt (θ_s) is the angle between the z axis and the vector connecting from the first atom to the last atom of the same chain. The molecular tilt (θ_m) is the average angle between the z axis and the average vector passing through the adjacent atoms in a given molecular chain. The difference between θ_s and θ_m reflects the extent of a trans state for a given molecular chain. It can be seen that the difference between θ_s and θ_m in the CH₃-SAMs was close to 1°, which indicated a zigzag conformation. In contrast, the OEG-SAMs showed larger conformational disorder, as listed in Table 1.

To further examine the conformation of molecular chains in the SAMs, the distributions of dihedral angles for the

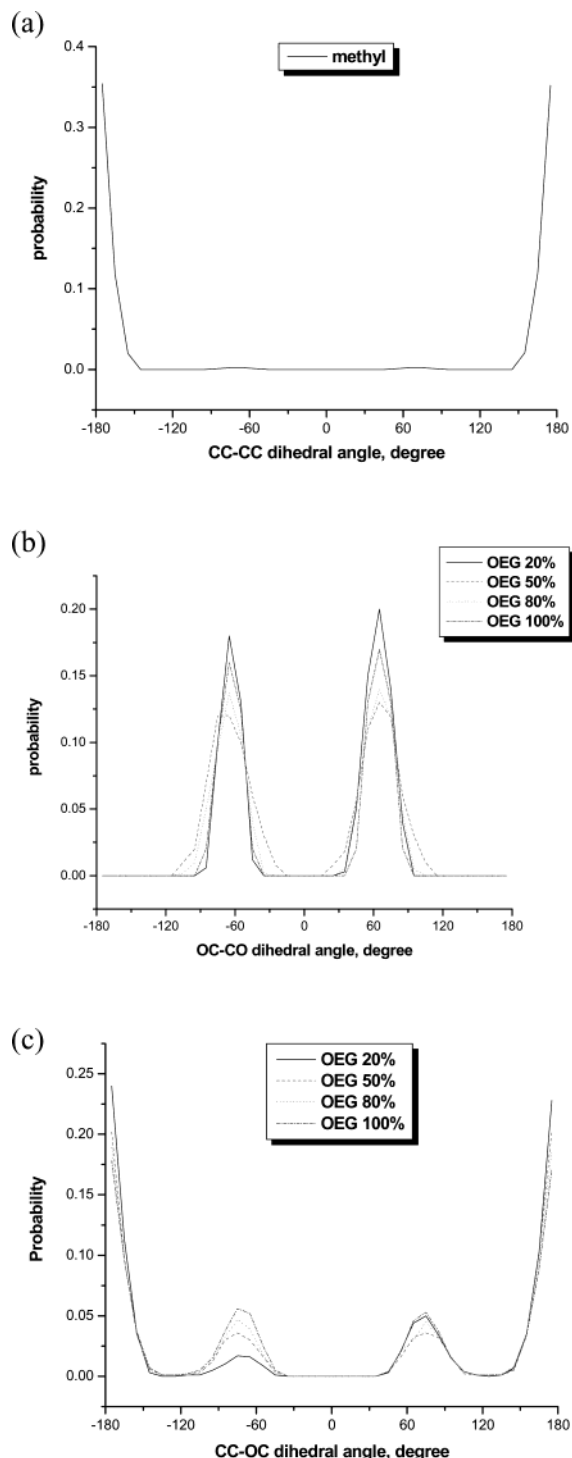


Figure 3. Probability distribution of the dihedral torsions for (a) the CC–CC torsion in the methyl-terminated SAMs, (b) the OC–CO torsion in the OEG-terminated SAMs, and (c) the CC–OC torsion in the OEG-terminated SAMs.

CH₃–SAMs and OEG–SAMs are shown in Figure 3. The CH₃–SAMs have one type of dihedral angle involving only heavy atoms, e.g. CC–CC, while the OEG portion of the OEG–SAMs has two types of dihedral angles, OC–CO and CC–OC. We define a trans dihedral angle corresponding to $\varphi = \pm 180^\circ$ and a gauche dihedral angle corresponding to $\varphi = \pm 60^\circ$. For the CH₃–SAMs, there were two sharp peaks for the CC–CC dihedral angles at $\pm 180^\circ$, indicating that this system has a zigzag conformation. For the OEG–SAMs, the distribution of the OC–CO torsions showed a large population of the gauche confor-

mation at $\pm 66^\circ$ (Figure 3b). This value was in good agreement with the value of 68° obtained from the wide-angle X-ray diffraction (WAXD) method.²⁹ Unlike the OC–CO angles, the distribution of the CC–OC dihedral angles exhibited both gauche (at $\pm 180^\circ$) and trans (at $\pm 66^\circ$) states in Figure 3c.

To further analyze the state of the SAMs, the percentage of trans and gauche conformations was calculated by integrating the probability distribution of the dihedral angle around $\pm 180^\circ$ and $\pm 66^\circ$ with a width of 15° , respectively. For the CH₃–SAMs, all CC–CC angles were found to be trans with an average trans angle of $\sim \pm 180^\circ$, which exhibited crystalline behavior. In the case of the OEG–SAMs, according to the WAXD data,²⁹ for crystalline PEG, all OC–CO dihedral angles are gauche and all CC–OC dihedral angles are trans. For amorphous PEG, the rotational isomeric state (RIS) model²⁹ shows that 80% of the OC–CO dihedral angles are gauche, while 73% of the CC–OC dihedral angles are trans. In this work, for the OC–CO dihedral angles, the gauche–trans ratios were 0.90:0.10, 0.73:0.27, 0.81:0.19, and 0.93:0.07 at $\chi_{\text{OEG}} = 0.2, 0.5, 0.8,$ and 1.0 , respectively. For the CC–OC dihedral angles, the gauche–trans ratios were 0.18:0.82, 0.21:0.79, 0.24:0.76, and 0.30:0.70 at $\chi_{\text{OEG}} = 0.2, 0.5, 0.8,$ and 1.0 , respectively. Thus, the OC–CO angles were found to favor a gauche form, whereas the CC–OC angles favor a trans form. As compared to the experimental results discussed above, the OEG–SAMs at $\chi_{\text{OEG}} = 0.5$ and 0.8 are close to an amorphous state while OEG–SAMs at $\chi_{\text{OEG}} = 0.2$ and 1.0 are in nonamorphous states.

The mobility of chains in various SAMs was monitored by the RMSD values. For the OEG–SAMs, the RMSD was calculated from both OEG- and OH-terminated chains. Among various OEG–SAMs, the mobility of chains was larger at $\chi_{\text{OEG}} = 0.5$ and 0.8 than at $\chi_{\text{OEG}} = 0.2$ and 1.0 . In the case of pure OEG–SAMs, the flexibility of the SAMs was reduced due to a high packing density. However, for the dilute 20% OEG–SAMs, a large amount of penetrating water molecules and OH chains stabilized the structure of OEG–SAMs, reducing the mobility of chains. At $\chi_{\text{OEG}} = 0.5$ and 0.8 , the large mobility of the OEG molecules was attributed to both molecular chain packing density and penetrating water molecules. It is interesting to note that the OEG–SAMs at $\chi_{\text{OEG}} = 0.5$ and 0.8 , which are in an amorphous state, also have higher mobility and less ordered molecular chains. In addition, we also compared the mobility of CH₃ chains with OEG chains. Results showed that RMSD was larger in the OEG–SAMs than in the CH₃–SAMs, indicating that the molecular chain of OEG was more flexible than those in the CH₃–SAMs.

Water Structure and Dynamics. Hydrogen bonding between water and the SAM surface also plays an important role in protein adsorption. Hydrogen bonds can be defined on the basis of either energetic or geometric criteria. In our study, we used the geometric criterion to determine hydrogen bonds. A hydrogen bond exists if the donor–acceptor distance is less than 0.35 nm and the hydrogen donor–acceptor angle is smaller than 60° . We analyzed the total number of hydrogen bonds between each oxygen atom in the OEG and OH chains and the water molecules. Results are listed in Table 2. For the CH₃–SAMs, there are no hydrogen-bonding acceptors available in the chains. For the OEG–SAMs, one can see that hydrogen bonds are formed around all oxygen atoms of the OEG chains. The total number of hydrogen bonds was larger at $\chi_{\text{OEG}} = 0.5$ and 0.8 than at $\chi_{\text{OEG}} = 0.2$ and 1.0 . For the pure OEG–SAMs (100%), the number of hydrogen bonds around each oxygen atom in OEG chains

Table 2. The Total Number of Hydrogen Bonds between Each Type of Oxygen Atom in the OEG and OH Chains and the Water Molecules for the System Box Used^a

| | OEG-SAMs | | | |
|-----------------|--------------|--------------|-------------|-------------|
| | 20% | 50% | 80% | 100% |
| O1 ^b | 14.6 ± 1.4 | 18.3 ± 1.9 | 7.5 ± 0.8 | 0.0 ± 0.0 |
| O2 ^b | 29.8 ± 2.1 | 42.7 ± 3.6 | 18.5 ± 1.8 | 0.0 ± 0.0 |
| O3 ^b | 29.3 ± 2.9 | 53.9 ± 4.4 | 17.8 ± 2.7 | 0.0 ± 0.0 |
| O4 ^b | 32.0 ± 2.7 | 58.6 ± 4.3 | 34.0 ± 2.6 | 1.1 ± 0.8 |
| O5 ^c | 75.5 ± 4.7 | 181.5 ± 7.6 | 250.5 ± 7.5 | 281.7 ± 8.6 |
| O ^c | 110.9 ± 7.1 | 59.0 ± 3.5 | 12.7 ± 1.0 | 0.0 ± 0.0 |
| total | 292.1 ± 11.6 | 414.0 ± 16.8 | 340.9 ± 9.3 | 282.8 ± 9.0 |

^a The total number of hydrogen bonds is counted for both the OEG and OH chains in the system. The error corresponds to the standard deviations. ^b The ethylene glycol oxygen atoms (O1–O4). The separation distance between oxygen atoms and the sulfur atoms increased as O4 > O3 > O2 > O1. ^c The hydroxyl oxygen atoms (O5 and O) in S(CH₂)₄(OCH₂CH₂)₄OH and in S(CH₂)₄OH, respectively.

was reduced due to high packing density. As the surface coverage of OEG-SAMs decreased to 20%, the number of hydrogen donors from the OEG-SAMs was also decreased. In this case, even though a large amount of water molecules penetrated into the OEG-SAM layers, only limited number of water molecules formed hydrogen bonds with OEG chains. The number of hydrogen bonds between water and OEG-SAMs depends on not only the number of penetrating water molecules but also the number of hydrogen donors available from OEG chains. As a result, the total number of hydrogen bonds around each oxygen atom in OEG chains exhibited peaks around $\chi_{\text{OEG}} = 0.5$ and 0.8 and was then reduced for the highly dense or dilute SAMs. In addition, as shown in Table 2, a relatively large amount of hydrogen bonds were observed around the hydroxyl oxygen atoms (O5). This also could be seen from the sharp, strong first peak of the radial distribution function in Figure 5.

Figure 4 showed a snapshot of hydrogen bonds for water molecules around an OEG chain. It can be seen that four water molecules form hydrogen bonds bridging between two adjacent oxygen atoms along the OEG chain. Similar bridging hydrogen-bonded structures were also observed in other simulation studies of PEG in solution.^{13,26,33} An additional two molecules were found to form single hydrogen bonds with the OEG chain. The rest of the water molecules, which were around the chain but did not form hydrogen bonds, were considered as free water (not shown in Figure 4). For the OEG-SAMs, water molecules inside the SAMs stabilized the helical conformation of chains.

To obtain a more detailed analysis of the structure of water at the interfaces, the radial distribution function (RDF) for the water molecules (O_{water}) around the end-group in each SAM chain, i.e., the last hydroxyl oxygen atom (O5) or the last CH₃-SAM carbon atom (C10), was illustrated in Figure 5. RDF is defined as

$$g_{ij}(r) = \frac{\langle N_{ij}(r) \rangle V(r)}{\rho_{j,bulk}}$$

where $\langle N_{ij}(r) \rangle$ is the ensemble averaged number of atom j in a spherical shell of volume $V(r)$ at a distance r from atom i , and $\rho_{j,bulk}$ is the bulk density of atom j . It should be pointed out that a spherical shell $V(r)$ may contain water, as well as protein and SAM chains. Thus, to obtain more accurate $g_{ij}(r)$, the local volume occupied by water molecules is calculated by subtracting the volume occupied by molecules other than water from a total spherical shell volume. Unlike calculations of $g(r)$ by a conventional method, this improvement allows us not to manually

rescale the tail of $g(r)$ to 1.0 at the longer distance. For the OEG-SAMs, a sharp, strong first peak was observed at 0.30 nm, corresponding to the nearest-neighbor distance between the OEG oxygen atoms and water. This peak position is consistent with the value of 0.29 nm reported in the Tasaki model.²⁶ The intensity of this peak is significantly higher than that in bulk water. This peak arises from strong interactions with nearby water molecules through hydrogen bonds. The second peak of the O_{water}-O5 RDF was around 0.50 nm and the third peak was around 0.75 nm. The width of these two peaks was much broader than that of the first peak. The separation of adjacent oxygen atoms of OEG chains is ~0.3 nm. These second and third peaks suggested that water molecules could penetrate deep into the OEG layer and form hydrogen bonds with oxygen atoms O4 and O3 of the OEG chains. For pure OEG-SAMs, $g(r)$ only showed the first two peaks and then approached to 1.0 as the distance between water molecules and OEG oxygen atoms (O5) was larger than 0.7 nm due to highly packing density. For 20% OEG-SAMs, more penetrating water molecules were confined between chains so that they made the second and third peaks higher in $g(r)$. Thus, the behavior of the $g(r)$ showed strong water clustering at the protein/SAM interface and a tightly bound water film at the top of the OEG units. Since water molecules wet the OEG-SAM surfaces, no water-preferred orientations with respect to the surfaces were observed. Figure 5 also showed the RDF for the methyl carbon atom and the nearby water oxygen atoms (diamond marked line). As expected, for the CH₃-SAMs, the position of the first peak in the RDF profiles was shifted to a larger distance of 0.41 nm, and no other pronounced peaks were observed. As can be also seen from snapshots of the CH₃-SAM system, there was a gap (~0.15 nm) between water molecules and the hydrophobic surface. Water molecules near the surface exhibited a preferred orientation, which lies parallel to the surface. Similar behavior of water molecules at the hydrophobic surface was reported in our previous work.^{31,32}

Figure 6 showed the distribution of water molecules along the z direction at the SAM interfaces in various protein/SAMs systems. The coordinates of sulfur atoms in the z direction are taken as the origin. For the OEG-SAMs, the water profiles generally have a similar shape. It can be seen from Figure 6 that a large amount of water molecules penetrated into the OEG portion of chains. The number of water molecules increased as surface coverage decreased, i.e., $\chi_{\text{OEG}} = 20\% > 50\% > 80\% > 100\%$. No water molecules were able to penetrate into the region of the alkane chain in the OEG-SAMs. For pure OEG-SAMs, one can see that water molecules cannot reach the level of the next to the topmost ethylene glycol oxygen atoms (O3). This observation is also confirmed by the fact that no hydrogen bonds form between water and O1–O3 atoms of the OEG chains, as shown in Table 2. It should be pointed out that more penetrating water molecules do not necessarily mean more hydrogen bonds formed. As we discussed above, the number of hydrogen bonds between water and OEG-SAMs depends on not only the number of penetrating water molecules but also the number of donors available from OEG chains. For the CH₃-SAM, the water profile showed a distinct shape.

Hypothesis of Protein Resistance. The experimental observation from Prime and Whitesides³⁵ showed that mixed SAMs of HS(CH₂)₁₁(CH₂CH₂O)₆OH and HS(CH₂)₁₀CH₃ appeared to adsorb protein (e.g., pyruvate kinase) as the mole fraction of HS(CH₂)₁₁(CH₂CH₂O)₆OH

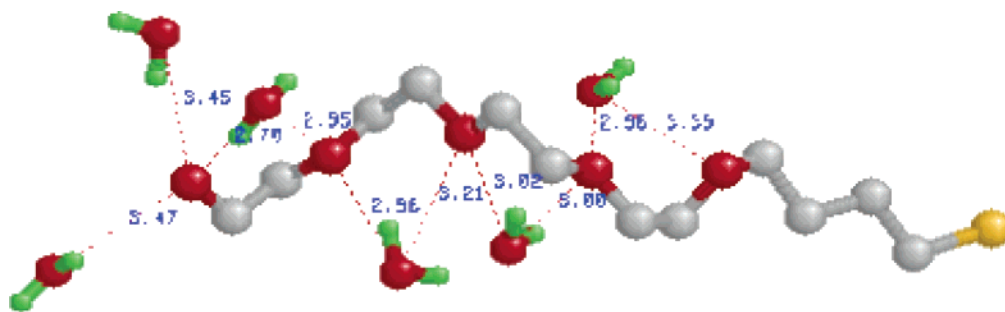


Figure 4. A representative instantaneous snapshot of a solvated OEG. Hydrogen bonds between water molecules and OEG oxygen atoms are marked through dashed lines with labeled distance. The color scheme is: OEG oxygen in green, OEG carbon in gray, water oxygen in red, and water hydrogen in light blue. OEG hydrogen atoms have been omitted for clarity.

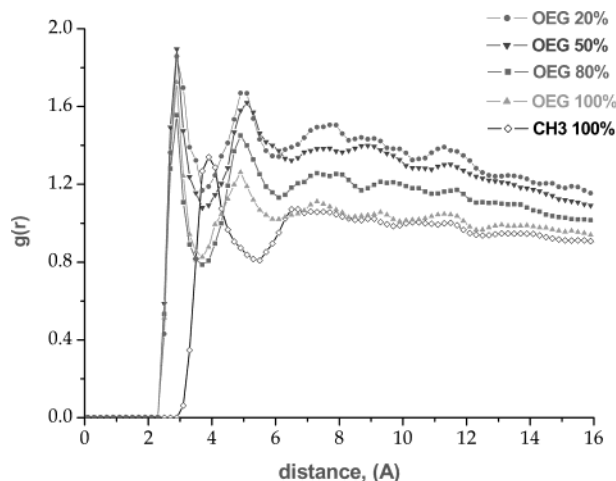


Figure 5. Radial distribution function, $g(r)$, of the water oxygen atoms around the OEG oxygen atoms and methyl carbon atoms.

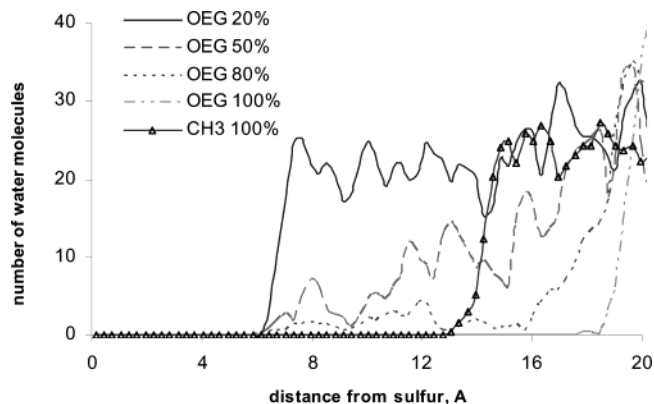


Figure 6. Distribution profiles for water along the z direction at the interfacial region for the OEG-SAM at $\chi_{\text{OEG}} = 0.2, 0.5, 0.8,$ and 1.0 and the CH_3 -SAM.

decreases to 0.5. Previously, OEG-SAMs were often prepared in ethanol solution. It has been shown that OEG-SAMs prepared from pure ethanol solution are not highly ordered and form incomplete monolayers.^{15,30} Our recent surface plasma resonance (SPR) experiments³⁶ show that the $\text{HS}(\text{CH}_2)_{11}(\text{CH}_2\text{CH}_2\text{O})_2\text{OH}$ and $\text{HS}(\text{CH}_2)_{11}(\text{CH}_2\text{CH}_2\text{O})_4\text{OH}$ SAMs assembled from mixed ethanol and water solution have a higher surface-packing density than those formed in ethanol solution and adsorb ~ 6 – 10% proteins, such as fibrinogen and lysozyme, as compared to less than $\sim 1\%$ in the case of OEG-SAMs formed in ethanol solution (Figure 7). In addition, Vanderah and

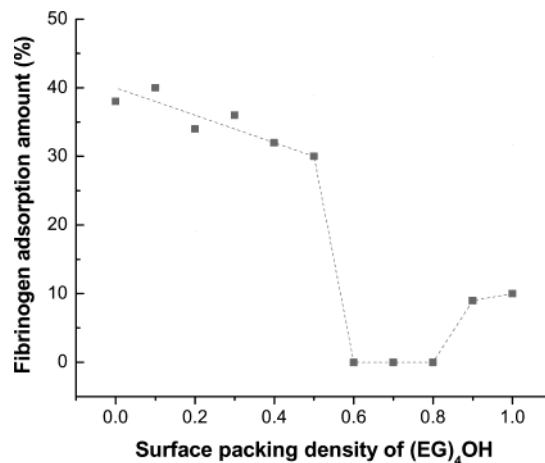


Figure 7. Fibrinogen adsorption amount versus the surface composition of $\text{HS}(\text{CH}_2)_{11}(\text{CH}_2\text{CH}_2\text{O})_n\text{OH}$.

co-workers³⁰ also showed that bovine serum albumin and lysozyme adsorbed to the most ordered, helical $\text{HS}(\text{OCH}_2\text{CH}_2)_6\text{CH}_3$ SAMs, but did not adsorb to the disordered $\text{HS}(\text{OCH}_2\text{CH}_2)_6\text{CH}_3$ SAMs. Therefore, on the basis of these experimental observations, for mixed OEG- and OH-SAMs, it is expected that these SAMs will resist protein adsorption within a certain range of surface OEG compositions, while it will adsorb proteins when its surface OEG density is too high or too low (Figure 7). In parallel, our simulation results from this work show that the total number of hydrogen bonds between water molecules and OEG chains is higher around $\chi_{\text{OEG}} = 0.5$ and 0.8 and decreases for densely packed pure OEG-SAMs or dilute mixed OEG-SAMs at $\chi_{\text{OEG}} = 0.2$. As compared with experimental results by Prime et al.³⁵ and us,³⁶ it appears that there is a correlation between the resistance of OEG-SAMs to protein adsorption and the amount of hydrogen bonds, i.e., the OEG-SAMs containing a large number of hydrogen bonds with water molecules have better non-fouling properties. Whitesides^{2,3} and Grunze^{13,14} suggested in their previous work that the formation of tightly bound water at interfaces is important in surface resistance to protein adsorption. Furthermore, our simulation results from RMSD of OEG chains show that those highly hydrated chains in mixed OEG-SAMs exhibit larger flexibility at $\chi_{\text{OEG}} = 0.5$ and 0.8 . As compared with experimental results by Prime et al.³⁵ and us,³⁶ it appears that there is a relationship between the mobility of OEG chains and nonfouling surfaces, i.e., those SAMs containing the high flexibility of OEG chains have better nonfouling properties. As suggested by Horbett and co-workers,¹ the high mobility of highly hydrated SAM chains leads to large OEG exclusion volume. For the CH_3 -SAM surface, in addition to less bound water molecules around

(36) Li, L.; Zheng, J.; Chen, S.; Ratner, B. D.; Jiang, S. *Langmuir*, submitted for publication.

chains and lower chain flexibility, the lack of any hydrogen-bonding capability of the CH_3 -SAM surface with water due to its nonpolar nature is a major factor for protein adsorption on the CH_3 -SAM surface.

In Gennes' steric repulsion model,⁹ the protein resistance to surfaces is mainly attributed to both elastic and osmotic effects. As a large protein approaches to a grafted "brush-like" PEO polymer layer, the elastic effect is caused by the compression of flexible PEO chains, yielding strong repulsive forces on the protein. The osmotic effect is caused by releasing tightly bound water molecules from the surface to the bulk, leading to an unfavorable energy penalty. Leckband and co-workers³⁷ proposed two modes (thermodynamic and kinetic control) of protein adsorption, depending on the characteristics of both the protein and the polymer brush. For small proteins, they can diffuse through the polymer brush by overcoming the kinetic energy barrier. This invasive mechanism favors primary adsorption on the surface corresponding to the kinetic control. For large proteins, they can only approach the surface by compressing the brush. This compressive mechanism favors secondary adsorption at the edge of the brush corresponding to thermodynamic control. We are currently performing molecular simulations to study the forces on a protein molecule exerted from OEG-SAMs and water molecules as the protein approaches the OEG-SAMs in order to directly evaluate the nonfouling properties of a surface from simulations.

IV. Conclusions

In this work, we performed a molecular simulation study of a system consisting of a protein (e.g., lysozyme) and

alkanethiolate SAMs terminating with different chemical groups [e.g., $(\text{OCH}_2\text{CH}_2)_4\text{OH}$, OH , and CH_3] in the presence of explicit water molecules and ions using a combination of MC and MD techniques. MC was used to determine the optimal orientation of the protein on SAM surfaces, while MD was used to investigate the dynamic behavior of SAMs, water molecules, and the protein. Our simulation results show that the total number of hydrogen bonds between water molecules and OEG chains is higher around $\chi_{\text{OEG}} = 0.5$ and 0.8 and decreases for either closely packed pure OEG-SAMs or dilute mixed OEG-SAMs at $\chi_{\text{OEG}} = 0.2$. Furthermore, our simulation results also show that, at $\chi_{\text{OEG}} = 0.5$ and 0.8, those chains in mixed OEG-SAMs exhibit larger flexibility from RMSD of OEG chains and are close to the amorphous state from the torsion distribution of OC-CO and CC-OC. In comparison with our recent SPR experimental results, it appears that there is a correlation between OEG surface resistance to protein adsorption and the amount of tightly bound water molecules around OEG chains (or the flexibility of hydrated SAM chains). That is, a large number of tightly bound water molecules around OEG chains or the high flexibility of OEG chains could be key factors for their nonfouling properties. This work provides useful molecular-level information toward a fundamental understanding of the nonfouling mechanism.

Acknowledgment. We thank Professor Buddy Ratner, Allan Hoffman, and Tom Horbett for helpful discussions. We gratefully acknowledge the National Science Foundation for financial support under CTS-0308598 and CTS-0092699. This work is also supported by a graduate research award to J.Z. from the Center for Nanotechnology at the University of Washington.

(37) Leckband, D.; Sheth, S.; Halperin, A. *J. Biomater. Sci., Polym. Ed.* **1999**, *10*, 1125.